Chromophore-Functionalized Glassy Polymers with Large Second-Order Nonlinear Optical Responses. Synthesis, Characterization, and Architecture-Processing-Response Characteristics of Poly(*p*-hydroxystyrenes) Functionalized with Chiral Chromophoric Side Chains

Millicent A. Firestone, Joonwon Park, Nobotsugu Minami, Mark A. Ratner,* and Tobin J. Marks*

Department of Chemistry and the Materials Research Center, Northwestern University, Evanston, Illinois 60208-3113

Weiping Lin and George K. Wong

Department of Physics and Astronomy and the Materials Research Center, Northwestern University, Evanston, Illinois 60208-3113

Received September 29, 1994[⊗]

ABSTRACT: This paper reports a systematic study of the synthesis, characterization, and second-order nonlinear optical properties of a series of chromophore-functionalized glassy polymers prepared by covalently appending chiral *N*-(4-nitrophenyl)-(*S*)-prolinoxy ((*S*)-NPP) moieties to poly(*p*-hydroxystyrene) (PHS). Key issues are how macromolecule architecture, chromophore–chromophore interactions, and processing (including corona and contact electric field poling) modulate second harmonic generation (SHG) efficiency as well as the temporal stability thereof. As probed by optical spectroscopy, optical rotation, FT-IR, homochiral versus racemic NPP substituents, and the dependence of SHG response on the chromophore number density, the effects of chromophore–chromophore interactions are found to be relatively minor for 16–90% functionalization of the PHS backbone. The nonresonant second harmonic coefficient, d_{33}, for corona-poled films varies from 12.8×10^{-9} to 79.0×10^{-9} esu ($\lambda = 1.064\ \mu$m) over this same functionalization range. The relationship of d_{33} and the contact poling field is approximately linear with the poling field up to ~1.3 MV/cm, beyond which saturation of the response is observed. Increasing NPP functionalization levels are accompanied by declining SHG temporal stability, which approximately tracks polymer T_g values. SHG temporal stability subsequent to poling can be substantially enhanced by prepole film annealing which removes volatile, plasticizing contaminants (and/or minimizes free volume) and by simultaneous cross-linking with diexpoxide reagents. For example, simultaneous poling and cross-linking of (*S*)-NPP–PHS films with 1,2,7,8-diepoxyoctane effects a 3-fold enhancement in the long-term time constant for SHG decay at 25 °C. However, the influence of various diepoxides on film transparency and SHG temporal characteristics is a sensitive function of stoichiometry and diepoxide conformational mobility. An accompanying contribution explores quantitatively how poling methodology influences macromolecular dynamics and SHG temporal stability.

The increasingly important role played by polymeric materials in numerous photonics technologies necessitates an improved understanding of macromolecular architecture–processing–property relationships. Of interest in this laboratory have been macromolecules designed to exhibit unusual second-order nonlinear optical (NLO) responses such as second harmonic generation (SHG), in which the frequency of incident radiation, ω, is efficiently doubled to 2ω.[1-10] The construction of efficient polymeric SHG materials requires maximization of the chromophore number density as well as the achievement and preservation of imposed microstructural noncentrosymmetry.

Second-order NLO polymers have successfully been prepared by incorporating chromophores of large molecular hyperpolarizability, β, into glassy polymer matrices. Removal of the macroscopic centricity is commonly accomplished by electric field poling, which involves simultaneously heating the polymer to near the glass transition temperature, T_g, and applying a dc electric field, thereby causing the dipolar chromophores to align preferentially with the field.[11] The earliest polymeric NLO materials were "doped" glassy polymers, in which the NLO chromophores were dispersed in the host matrix.[11-14] These materials suffer, to varying degrees, from three serious limitations: (i) generally low attainable chromophore concentrations (due to thermodynamically imposed solubility restrictions); (ii) compositional/thermal/chemical instability (due to weak binding of the chromophores within the matrix); and (iii) loss of the electric field-imposed chromophore alignment; hence, SHG efficiency (due to the relatively high rotational mobility of the unconstrained chromophore molecules within the matrix environment).[15] Significant improvements in properties have been achieved by covalently linking the NLO chromophore to the backbones of high-T_g glassy polymers.[11,16-22] This design modification substantially increases the achievable chromophore number densities, enhances compositional/chemical stability, and impedes chromophore reorientation. To date, the majority of studies on side-chain chromophore-functionalized NLO polymers have centered on relatively mobile methacrylate polymers and derivatives thereof.[11,20,23-28] Fewer reports have discussed the synthesis and properties of materials employing alternative, potentially less mobile polymer backbones.[11,16,18,22,29-33] Although several styrene-based polymer systems have been reported,[11,16,29] there have been no *systematic, in-depth* examinations of the influ-

[⊗] Abstract published in *Advance ACS Abstracts,* February 15, 1995.

0024-9297/95/2228-2247$09.00/0

ence of various polymer architectural characteristics or processing methodologies on the NLO efficiency and relaxation properties for such functionalized polymers.

In this paper, we present a full account of the synthesis, characterization, and second-order NLO properties of a model side-chain, chiral chromophore-functionalized polymer consisting of *N*-(4-nitrophenyl)-(*S*)-prolinoxy covalently bound to poly(*p*-hydroxystyrene) ((*S*)-NPP–PHS; **I**). Specifically, we examine the impact

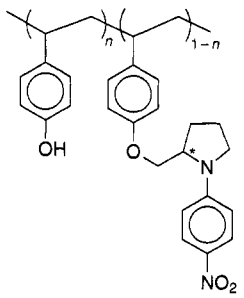

I

of chromophore functionalization level and prepoling processing on SHG efficiency and SHG relaxation characteristics. We also investigate the possible presence of detrimental centrosymmetric chromophore–chromophore aggregation, using several spectroscopic probes. In addition, we investigate in detail the consequences of simultaneously poling and cross-linking the matrix as a means of preserving maximum acentricity, and thereby modifying SHG temporal characteristics.

N-(4-Nitrophenyl)-(*S*)-prolinol (NPPOH) was selected for three reasons. First, it possesses a chiral center which should resist centrosymmetric aggregation[34] of the chromophore substituents. Additionally, the chiral center serves both as an easily monitored spectroscopic "marker", indicating the level of functionalization, and as a probe of the extent of chromophore aggregation. Second, the chromophore possesses hydrogen-bonding sites ($-NO_2$) which, by interacting with the phenolic polymer matrix, could potentially stabilize the electric field-induced chromophore alignment. Finally, NPPOH exhibits high chemical and thermal stability and photostability. Poly(*p*-hydroxystyrene) (PHS; also called poly(4-vinylphenol)) was selected for the relatively high glass transition temperature (155–180 °C, evidence of low conformational mobility), extensive hydrogen-bonding capacity, good film-forming characteristics, robust chemical/thermal characteristics, amenability to straightforward functionalization, and ready availability of samples having well-defined molecular weights.[35–37]

In the accompanying paper,[38] we build upon this synthetic/microstructural information base and explore how details of the electric field poling methodology (*i.e.*, variation of poling time/physical aging, temperature, and poling field strength) further modulate macromolecular dynamics and SHG temporal characteristics.

Experimental Section

Physical Methods. UV–visible absorption spectra were recorded using a Perkin-Elmer Model 330 spectrophotometer. FT-IR spectra were collected on a Matteson Alpha Centauri spectrometer. ^{1}H NMR spectra were recorded on either a JEOL FX-270 (270 MHz) or Varian XL-400 (400 MHz) spectrometer. Specific optical rotation measurements were made using an Optical Activity Ltd. AA-100 polarimeter. Elemental analyses were performed by G. D. Searle Inc. (Skokie, IL). Thermal properties of the (*S*)-NPP–PHS polymers were measured by DSC (10 °C/min heating rate; instrument calibrated using polystyrene or indium standards) on either Perkin-Elmer DSC-2 or DSC-7 instruments. The glass transition temperature, T_g, was defined as the midpoint of the transition (Table 1). X-ray diffraction data were collected on a Rigaku Geigerflex diffractometer using Ni-filtered Cu Kα radiation. The density of 90% functionalized (*S*)-NPP–PHS was determined by flotation in aqueous solutions of zinc chloride.[39,40] Only the 90% functionalized copolymer could be studied by this technique due to the hydrophilicity of the materials with lower functionalization levels. Film thicknesses were determined after SHG measurements with an α-step stylus profilometer (Tencor Instruments).

Table 1. Dependence of Glass Transition Temperature on Functionalization Level for (*S*)-NPP–PHS Polymers

functionalization level[a] (%)	glass transition temp, T_g[b] (°C)	functionalization level[a] (%)	glass transition temp, T_g[b] (°C)
0	155	48	112
12	146	62	106
36	134	90	96

[a] As determined by elemental analysis. [b] Defined as the midpoint of the transition.

The indices of refraction of 36% functionalized (*S*)-NPP–PHS polymer films were measured by spectroscopic ellipsometry[41] (SOPRA multilayer optical spectroscopic scanner, Model ES-4G). Data were collected on an unpoled 2.87-μm-thick film which was cast in standard fashion onto an ITO–glass substrate. The underside of the glass was painted black to prevent the incident light from reflecting off the bottom interface, thereby confining the rays to the air/polymer/ITO–glass multilayer. Tan Ψ and cos Δ data (31 points) were collected at an incident angle of 55° between 0.500 and 0.800 μm (0.01 μm intervals) using a Hadamard transform of the photodetected signal. The ITO–glass layer was measured independently, allowing the entire assembly to be modeled as a three-layer (air/polymer/substrate) structure. The collected data were fit to the Sellmeir equation[41–43] to obtain (by extrapolation) the refractive indices over the range of wavelengths between 0.530 and 1.064 μm (a range encompassing the λ of the fundamental probe beam and the measured second harmonic).

Synthesis of *N*-(4-Nitrophenyl)-(*S*)-prolinoxy Tosylate. Modifications of literature methods were used to synthesize *N*-(4-nitrophenyl)-(*S*)-prolinol (NPPOH)[44,45] and the tosylate derivative thereof (NPPOTs).[46] A Schlenk flask charged with (*S*)-NPPOH (4.0 g, 18.0 mmol) in pyridine (50 mL) was stirred under N_2 to give a clear yellow solution. After cooling to 0 °C, *p*-toluenesulfonyl chloride (Aldrich; 6.86 g, 36 mmol) was slowly added so as to maintain the temperature below 3 °C. The clear yellow solution was stirred for 1 h at 0 °C and then placed in a refrigerator overnight. The solution was next poured into ice water (350 mL) to precipitate the chromophore tosylate. The resulting yellow precipitate was collected by suction filtration, washed with ice water (250 mL), and dried under vacuum. Analytically pure product was obtained by recrystallization by diffusion of cyclohexane into chloroform solutions. Anal. Calcd for $C_{18}H_{20}N_2O_5S$: C, 57.43; H, 5.36; N, 7.44. Found: C, 57.25; H, 5.34; N, 7.44. ^{1}H NMR ($CDCl_3$): δ 2.07 (br, 4H), 2.40 (s, 3H), 3.23 (m, 1H), 3.42 (m, 1H), 3.87 (m, 1H), 4.04 (m, 1H), 4.07 (br, 1H), 6.39 (d, J = 9 Hz, 2H), 7.27 (d, J = 8 Hz, 2H), 7.70 (d, J = 8 Hz, 2H), 8.01 (d, J = 9 Hz, 2H).

Synthesis of *N*-(4-Nitrophenyl)-(*S*)-prolinoxy-Functionalized Poly(*p*-hydroxystyrene) Polymers. The chromophore was appended to PHS (M_W = 5800) by one of two related procedures (A and B). In a representative example using method A, poly(*p*-hydroxystyrene) (PHS; 1.00 g, 8.32 mmol of repeat units) and sodium hydroxide (0.33 g, 8.25 mmol) were stirred under N_2 in N_2-saturated distilled water (50 mL) at room temperature to give a clear brown solution. After addition of (*S*)-NPPOTs (2.82 g, 7.49 mmol), the mixture was stirred at 90 °C overnight. The resultant precipitate was collected by suction filtration, washed with water (300 mL), and dried under vacuum. Unreacted (*S*)-NPPOH and (*S*)-

Table 2. Elemental Analyses of (*S*)-NPP-PHS Polymers at Various Functionalization Levels

functionalization level (%)	theoretical (%)			experimental (%)		
	C	H	N	C	H	N
12	77.39	6.57	2.32	76.70	7.05	1.91
16	76.70	6.54	2.93	76.30	7.01	2.50
48	73.11	6.36	6.16	73.28	6.68	6.16
36	74.17	6.41	5.21	73.99	6.74	5.06
62	72.13	6.31	7.06	72.35	6.54	7.06
75	71.41	6.27	7.69	71.15	6.48	7.46
90	70.73	6.23	8.29	70.15	6.69	7.90

NPPOTs were removed by repeated dissolution of the yellow polymeric powder in a small quantity of THF and precipitation by dropwise addition to benzene. Final purification of the product was by chromatography on a silica gel column with THF as the eluent. A brown powder (0.96 g; 48% of phenol groups functionalized as assayed by elemental analysis based upon N content (yield = 47%)) was obtained by a final precipitation from THF with benzene, followed by drying under vacuum.

In method B, a Schlenk flask charged with PHS (0.12 g, 1.00 mmol of repeat units) and sodium hydride (Aldrich; 48 mg, 12.0 mmol) was evacuated and then back-filled with N_2. Distilled 1-methyl-2-pyrrolidone (NMP; Aldrich; 5 mL) and (*S*)-NPPOTs (0.75 g, 2.0 mmol) were added, and the mixture was stirred for 1 h at 100 °C to yield a red–brown solution. After cooling, the solution was added dropwise to distilled water (50 mL) to precipitate the solid polymer. The crude product was collected by filtration, washed with water, and dried under vacuum. The dried powder was then dissolved in THF and poured onto silica gel. Evaporation of the THF left a coating of the crude yellow product on the silica gel. This coated gel was subsequently placed atop a silica gel column, and unreacted organics were eluted with diethyl ether. Subsequent elution with THF provided the pure functionalized polymer. Isolation of the product was achieved by precipitation from cyclohexane (210 mg, 0.69 mmol, 90% of phenol groups functionalized as assayed by elemental analysis based upon N content (yield = 69%)). Subsequent purification followed the procedure described above. In Table 2 are compiled the results of the elemental analyses for the various levels of functionalized polymer employed in this study.

Fabrication of Polymer Films. Polymer films were prepared by dissolution of the polymer powder (ca. 10 mg/mL) in freshly distilled (from Na/K) THF, followed either by gravity filtration or by filtration through a 0.5 μm syringe filter. The solutions were then cast onto clean indium tin oxide (ITO)-coated glass substrates in a laminar flow class 100 clean hood. After slow evaporation of solvent at room tempeature, the films were annealed at 150 °C under vacuum overnight to ensure removal of solvent.

Corona Poling with in-Situ SHG Monitoring. The ITO–glass substrates coated with the annealed (*S*)-NPP–PHS films were affixed to an aluminum plate (5.08 × 5.08 cm) having a 1.27 cm hole, through which the incident laser beam was directed. Between this plate and an identical plate were attached a thermofoil heater (Minco Co.) and a K-type thermocouple (Figure 1A). The thermocouple was calibrated in an independent experiment to read the temperature of the polymer. This assembly was secured on the optical bench in a stage, the position of which was optimized using a He–Ne laser. The stainless steel corona needle was positioned normal to the film surface with a needle-to-film separation of 1.0 cm.[47] All poling studies were conducted in an ambient atmosphere. The corona voltage (+3 to +5 kV) was maintained using a high voltage dc power supply (Spellman), while the sample was heated to the desired temperature. Upon saturation of the SH signal intensity, the sample was slowly cooled to room temperature. Once room temperature was reached, the poling field was terminated. Films were stored in a desiccator for the duration of decay studies.

Contact Poling with in-Situ SHG Monitoring. The annealed (*S*)-NPP–PHS films were contact poled with *in-situ* SHG monitoring, using the configuration shown in Figure 1B.

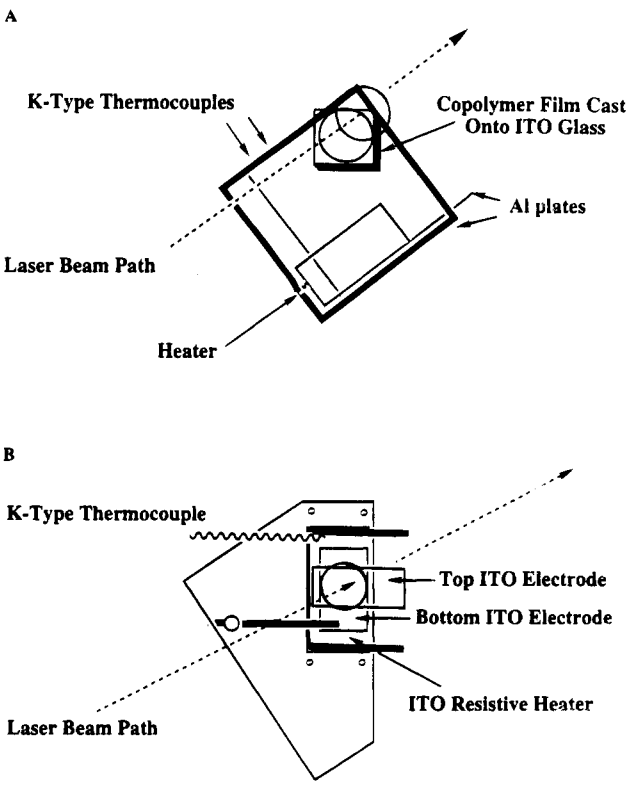

Figure 1. (A) Schematic of the apparatus for corona poling with *in-situ* monitoring of the SHG signal. (B) Schematic of the apparatus for contact poling with *in-situ* monitoring of the SHG signal.

This arrangement features two transparent ITO electrodes between which the polymer film is sandwiched. The ITO/polymer film assembly is then secured in the polycarbonate holder (Figure 1B) which had a 1.27 cm hole, through which the incident laser beam was directed. Heating was provided by an ITO resistive heater with an appended K-type thermocouple. In an independent experiment, the thermocouple was calibrated to reflect the true sample temperature using temperature indicating paints (Omega Engineering Inc.), which were placed in the same location and configuration as the polymer film during *in-situ* analysis. The poling circuit included attachment of the ITO electrodes to an external dc power supply (Kepco) and a picoammeter (Keithly 485), which served to monitor current flow through the sample throughout the duration of *in-situ* poling. During all phases of the poling process, currents remained in the nanoampere range. No evidence was found for abrupt jumps in the SHG signal intensity upon applying or terminating the poling field ("switching effects").[15e]

Second-Harmonic Generation Measurements. Second harmonic generation measurements were carried out with a Q-switched Nd:YAG laser (Quanta-Ray, DCR-1) operating at 1.064 μm in the p–p polarized geometry. The pulse width was less than 10 ns, and the repetition rate, 10 Hz. A quartz reference, which also monitored the laser power, and the sample were measured simultaneously throughout the course of experiments. The instrumentation and calibration techniques are more fully described elsewhere.[16] In accord with the static statistical–mechanical model for dipolar alignment in an external electric field,[12,48] the d_{33} and d_{31} tensor equations were found to be valid under the present corona poling conditions. In particular, it was found that over a wide range of processing conditions $d_{33}/d_{31} = 3.0 \pm 0.5$ using both accepted measurement methodologies—multiple-angle scanning and polarization-dependent SHG. A detailed experimental and theoretical account of this work will be discused elsewhere.[48b] The reproducibility in $I^{2\omega}$ values is estimated to be ±10%.

Simultaneous Poling and Thermal Cross-Linking. The diepoxide cross-linking reagents, (±)-1,3-butadiene diepoxide (**II**; 97%), 1,2,7,8-diepoxyoctane (**III**; 97%), and 1,4-

Scheme 1. Routes to Chromophore-Functionalized Poly(*p*-hydroxystyrenes)

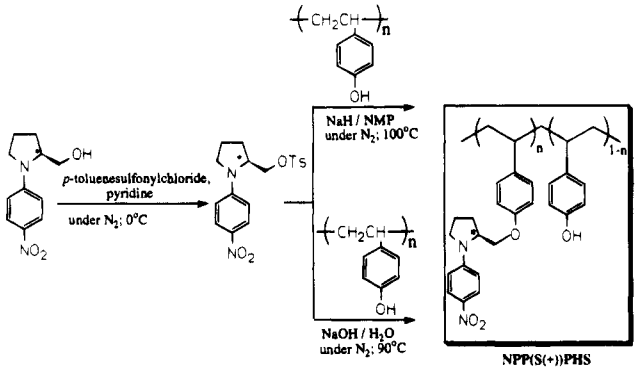

butanediol diglycidyl ether (**IV**; 95%), were obtained commercially (Aldrich) and used without further purification. Films for cross-linking studies were prepared by solvent casting in the standard fashion (*vide supra*) from THF solutions that contained the functionalized polymer and the selected diepoxide cross-linking reagent. Optimum conditions for cross-linking were established in independent experiments by FT-IR spectroscopy conducted with films on KBr plates (*vide infra*). The films were partially cured at 100 °C for 1 h under an inert atmosphere followed by continued heating (100 °C) under vacuum (10^{-4} Torr) for 24 h. The precured and annealed films were then corona poled using the apparatus and configuration detailed above. The corona voltage (+3 to +5 kV) was maintained, while the sample was heated to 180 °C. Upon saturation of the SH signal intensity (~1 h), the sample was cooled to room temperature. Once room temperature was reached, the poling field was terminated. Films were stored at room temperature in a desiccator for the duration of the decay studies.

Results and Discussion

We first describe two approaches to the synthesis of (*S*)-NPP–PHS polymers having a wide range of functionalization levels. Physicochemical studies then focus on polymer properties and potential chromophore–chromophore interactions employing a variety of spectroscopic techniques (linear optical, optical rotation, FT-IR, and SHG). The processing of this material, to preserve maximum acentricity, is investigated by development of an annealing protocol and implementation of *in-situ* epoxide cross-linking of the polymer matrix.

Polymer Synthesis. A random copolymer of poly(*p*-hydroxystyrene) (PHS) functionalized with 4-nitrophenyl-(*S*)-prolinol (NPPOH) was prepared from the corresponding tosylate (NPPOTs), by either of two methods. Both involve the attachment of the NPP chromophore to the polymer backbone via an ether linkage (Williamson ether synthesis).[49] The first of these procedures is carried out in an aqueous solution under alkaline conditions (Scheme 1). This approach is, however, suited only for the preparation of materials functionalized to levels less than ~62%. At higher chromophore loadings, the functionalized polymers have a limited solubility in the aqueous solution, so that further reaction is inefficient. This problem may be easily overcome by using an alternate method (Scheme 1), involving sodium hydride in nonaqueous media (1-methyl-2-pyrrolidinone; NMP).

Polymer and As-Cast Film Characterization. Elemental analysis served as the primary method for determining the chromophore functionalization level. As shown in Table 2, the experimental C, H, and N values all agree to within ±0.4% of the calculated values, reflecting the high purity of the copolymers. The 400-MHz ^{1}H NMR spectra of the polymers are not structurally definitive, exhibiting only broad resonances. They indicate, however, that the concentration of free, low molecular weight organics is below the detection limit. Determination of the chromophore number densities of the (*S*)-NPP–PHS samples requires knowledge of the macroscopic densities. The density of a 90% chromophore-functionalized polymer sample was determined experimentally by flotation in an aqueous zinc chloride solution.[40,41] A density of 1.27 ± 0.01 g cm^{-3} was found, which agrees favorably with 1.29 g cm^{-3} estimated from the weighted average of the known densities of PHS (1.163 g cm^{-3})[50] and NPPOH (1.36 g cm^{-3}).[45]

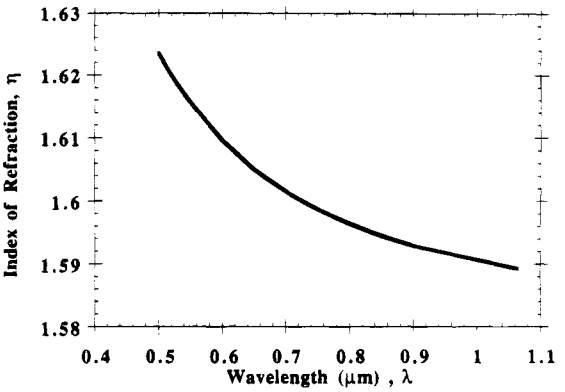

Figure 2. Wavelength dependence of the refractive index for a 36% functionalized (*S*)-NPP–PHS film as determined by spectroscopic ellipsometry. The solid curve represents refractive indices obtained by fitting experimental tan Ψ and cos (Δ) data to the Sellmeir equation.

The refractive index, as measured by spectroscopic ellipsometry on an as-cast 36% functionalized (*S*)-NPP–PHS film, increases monotonically from 1.589 at 1.064 μm to 1.618 at 0.532 μm (Figure 2). The index of refraction of the neat PHS polymer is reported to be 1.60 at the Na D line (0.589 μM).[50] This result and previous results for (*S*)-NPP–PPO[16c] indicate that the polymer index of refraction changes little with NPP functionalization. The derived index values compare well with similar values reported for other donor–acceptor chromophore-functionalized styrene polymers.[24] In regard to (*S*)-NPP–PHS linear optical properties, (*S*)-NPP exhibits a strong, broad charge-transfer (CT) absorption band at 390 nm ($\epsilon = 4.07 \times 10^4$ mol^{-1} cm^{-1}) in a THF solution. This energy of this excitation is in accord with theoretical calculations carried out using the ZINDO/SOS formalism,[51,52] which predicts a single dominant CT process, with a charge redistribution from the prolinol nitrogen to the π-accepting NO_2 functionality at λ_{max} = 337 nm.[53] Upon attachment of NPP to the PHS backbone, the optical maximum shifts to a slightly shorter wavelength in THF solution, 386 nm. This shift is accompanied by the appearance of a band at 280 nm, arising from the PHS π system (Figure 3). The energies of these solution-phase transitions are insensitive to the PHS functionalization level. The possibility of employing optical data for determining the degree of functionalization and detecting possible chromophore–chromophore interaction/aggregation effects was also explored. A reasonably linear relationship is found between the 386 nm absorbance and the chromophore concentration (Figure 4) for a wide range of functionalization levels examined (12–62% functionalized (*S*)-NPP–PHS). Some slight departure from linearity may be present at the highest level of functionalization (90%), possibly reflecting a minor association of the

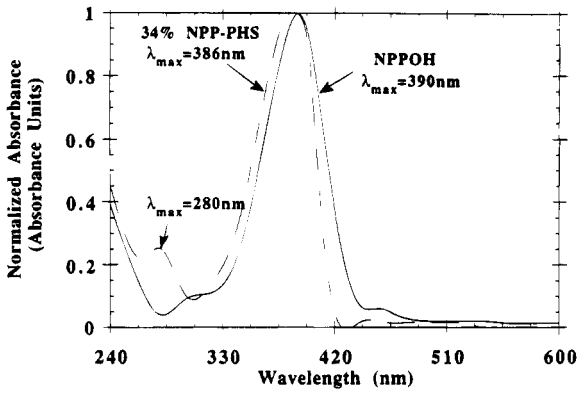

Figure 3. Comparison of UV–visible absorption spectra of 34% (*S*)-NPP–PHS in THF solution (dashed curve) to pure chromophore (*S*)-NPPOH in THF solution (solid curve). Data have been normalized to the absorption peak maximum.

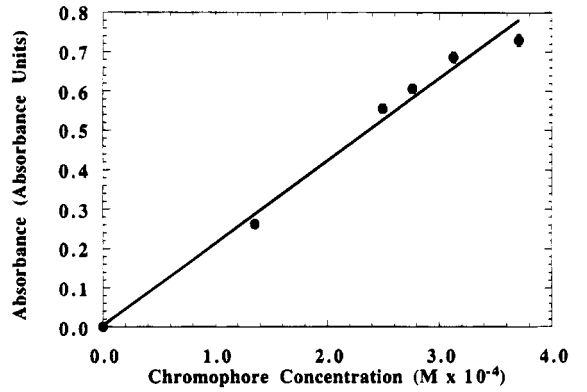

Figure 4. Absorbance (measured at the principal charge-transfer band associated with the appended chromophore, λ_{max} = 386 nm) as a function of chromophore concentration for (*S*)-NPP–PHS samples in THF solution. The line represents a least-squares fit to Beer's law.

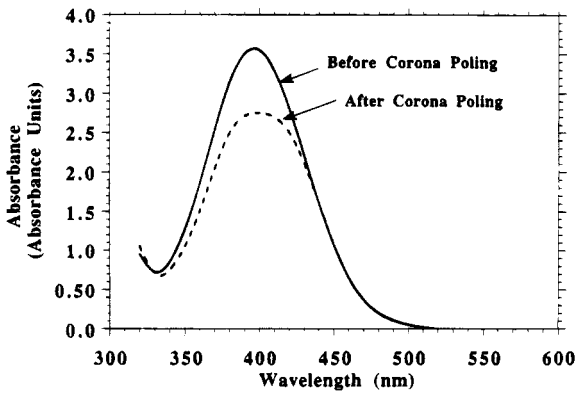

Figure 5. Transmission optical spectrum of a 48% (*S*)-NPP–PHS film before and after corona poling.

chromophore substituents at high concentrations;[54] however, extensive aggregation seems unlikely, since no significant alteration in either the energy or line shape of the NPP CT excitation band is observed over the full range of functionalization levels. These optical spectroscopic results are in good agreement with functionalization levels determined by elemental analysis. In Figure 5, the optical spectrum for a 48% functionalized (*S*)-NPP–PHS thin film (λ_{max} = 397 nm) (cast from THF and annealed under vacuum overnight at 120 °C) is shown. A red shift of ~11 nm is observed in the film chromophore absorption band versus THF solutions. It can be ascribed to small changes in chromophore–chromophore interactions, chromophore matrix hydrogen bonding, and/or to environmental polarity (solvatochromic) effects. In NPP–PHS films, the λ_{max} and line shape of this CT feature are essentially invariant with the NPP functionalization level. Importantly, it can also be seen from these data that the (*S*)-NPP–PHS film linear optical absorption maximum is far removed from the 532-nm 2ω light generated in the SHG experiments (*vide infra*) and that chromophore absorption has essentially reached "base line" by 520 nm. Thus, negligible resonant enhancement of the NLO response and negligible photochemical damage of the chromophoric substituent is anticipated (none is observed).[55] The same argument applies to possible film heating effects.[15e]

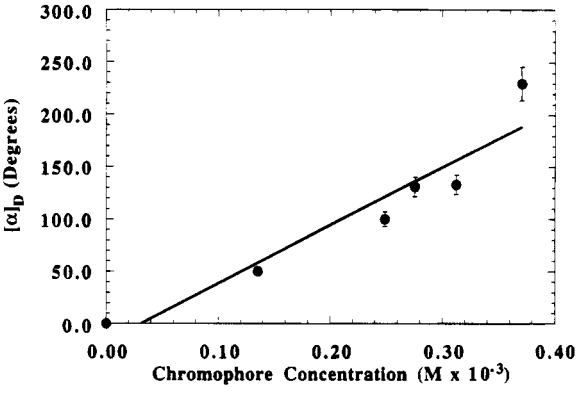

Figure 6. Specific rotation as a function of chromophore concentration of (*S*)-NPP–PHS in THF solution. The straight line is the linear least-squares fit to the experimental data.

Since the NPP chromophore has a chiral center, increased optical activity is expected upon increased PHS functionalization. Therefore, optical rotation was also investigated as a function of the level of chromophore substitution. As shown in Figure 6, an approximately linear relationship between optical rotation and chromophore concentration obtains over the range 12–62% functionalization. At the highest functionalization level (90%), however, some deviation from linearity is observed. This may again reflect chromophore association at high loadings.[55] In terms of synthetic chemistry, these results also demonstrate that the reaction conditions required for attachment of the chiral NPPOH chromophore to the polymer backbone do not incur significant racemization.

A transmission FT-IR spectrum of an unannealed 36% (*S*)-NPP–PHS film cast from a THF solution is presented in Figure 7. Characteristic vibrational modes include a broad, strong transition due to a distribution of the hydrogen-bonded polymeric alcohol functionalities (3362 cm^{-1})[57-61] and characteristic modes of the nitro group at 1518 (strong, sharp) and 1308 cm^{-1} (very weak).[57-61] Note that, in strongly associated polymers such as PHS, a narrower band associated with "free" (*i.e.*, non-hydrogen-bonded) hydroxyl groups is also typically observed at ca. 3525 cm^{-1}.[59] In the unannealed sample of 36% functionalized (*S*)-NPP–PHS, a small shoulder is, in fact, observed in this region, indicating that a small fraction of the hydroxyl groups present are free. Two (*S*)-NPP–PHS absorption bands absent in the infrared spectra of the pure NPPOH chromophore and the PHS polymer are observed at 1214 (sharp, moderate) and 1014 cm^{-1} (very weak) and are reasonably assigned to the ether linkage produced upon functionalization.[57-61] The FT-IR spectrum of the unannealed sample also exhibits two peaks at 1048 and 889 cm^{-1}, which arise from the presence of residual casting

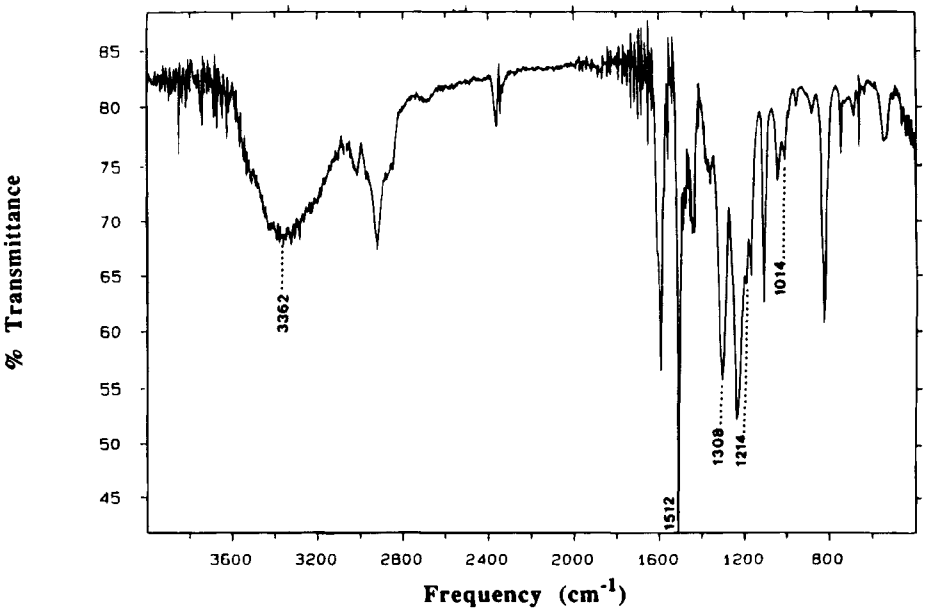

Figure 7. FT-IR spectrum of a 36% (*S*)-NPPOH functionalized PHS film with characteristic absorption bands indicated (full explanation provided in the accompanying text).

solvent, THF. Film FT-IR spectra as a function of increasing the (*S*)-NPP–PHS functional level reveal a progressive diminution in the intensity of the ν_{OH} region and displacement to higher frequency, indicative of a weakening of the hydrogen-bonding network. Increases in the NPP-centered transitions are also observed as expected. In view of the satisfactory (*S*)-NPP functionalization level information obtained from elemental analysis and optical spectroscopic data (*vide supra*), further quantitative analysis of the film FT-IR data (which has inherent quantitative limitations[61b]) was considered unnecessary.

Table 1 presents (*S*)-NPP–PHS T_g data as a function of the chromophore content. The data show a monotonic fall in T_g with increasing functionalization level. This diminution in T_g with side-chain functionalization is typical of random copolymers of amorphous morphology exhibiting a single T_g intermediate between the T_g's of the constituent monomer units. This empirical relationship is given in eq 1,[62]

$$\frac{1}{T_g} = \frac{M_a}{(T_g)_a} + \frac{M_b}{(T_g)_b} \qquad (1)$$

where the copolymer T_g is related to the mass fractions, M_a and M_b, and the T_g's of the respective comonomer units. As shown in Figure 8, the experimentally determined (*S*)-NPP–PHS glass transition temperatures conform well to eq 1. It will be seen that these mobility characteristics have significant consequences for the temporal stability of poling-induced chromophore alignment.

Film Processing. An annealing procedure was found necessary to remove solvent (THF) and other extraneous volatiles which deleteriously plasticize the polymer matrix.[62] FT-IR spectroscopy was used to monitor the removal of residual THF from the cast (*S*)-NPP–PHS films by following the reduction or disappearance of the characteristic 1048 and 887 cm^{-1} THF modes.[60] After heating at 100 °C under vacuum (10^{-4} Torr) for 2 h, both the 1048 cm^{-1} absorption and the 877 cm^{-1} band have been reduced in intensity, the latter significantly. Further heating to 150 °C reduces the

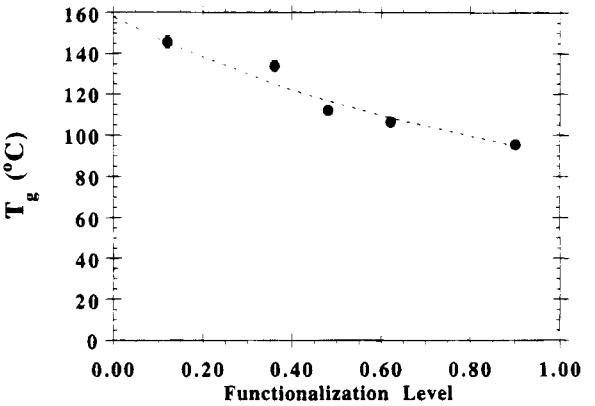

Figure 8. Effect of percent PHS functionalization on the glass transition temperature, T_g, for (*S*)-NPP–PHS. T_g is defined and taken as the midpoint of the DSC transition. The dotted line corresponds to the values expected from empirical eq 1.

1048 cm^{-1} band still further and effectively eliminates the 887 cm^{-1} band. Based upon these results, the solvent-cast films were annealed at 150 °C overnight under vacuum to assure complete removal of THF.

Poling Procedures and Properties of Poled (*S*)-NPP–PHS Films. The second-order nonlinear optical properties of the (*S*)-NPP–PHS copolymer films were examined simultaneously with poling by second harmonic generation (SHG) techniques. The SHG coefficient, d_{33} ($1/2\chi^{(2)}_{zzz}$), was determined from the film thickness and the second harmonic signal intensity relative to a quartz reference. Film absorption corrections were not applied since minimal optical absorption is detected at either the fundamental (1064 nm) or at the second harmonic (532 nm) wavelength (cf. Figure 5). No SHG signal is observed from unpoled samples.

Corona poling[47] was the primary technique employed in this study to induce acentricity/chromophore alignment in the (*S*)-NPP–PHS films. It was preferred to conventional contact electrode poling because it is less sensitive to local defects in the film surface which lead to dielectric breakdown and short-circuiting during contact poling.[63] Hence, larger field strengths are achievable, limited theoretically only by the intrinsic

Table 3. Effect of Functionalization Level on Second-Order Nonlinear Optical Coefficient, d_{33}, for Corona-Poled (S)-NPP-PHS Films

functionalization level (%)	d_{33}[a] (10^{-9} esu)	polymer density[b] (g/cm^3)	chromophore number density (10^{20}/cm^3)
16	12.8	1.18	7.68
36	44.5	1.20	13.3
48	58.4	1.21	16.0
62	65.7	1.23	18.7
75	71.5	1.24	20.5
90	79.0	1.26	22.5

[a] Measurements made at λ = 1064 nm fundamental. [b] Values for 16–75% functionalized samples were approximated via interpolation.

dielectric strength of the polymer. The protocol for (S)-NPP–PHS films consisted of poling at elevated temperatures (*e.g.*, in the vicinity of T_g) until a steady-state *in-situ* SHG signal intensity was achieved and then slowly cooling the sample to room temperature, after which time the electric field was terminated. The possibility of retention of residual charge after corona poling was examined by comparing the NLO characteristics of untreated poled polymer films to poled films swabbed with H_2O (which acts to hasten recombination/neutralization or surface charge).[18] The results demonstrate that, under the prevailing experimental conditions (*i.e.*, humidity, sample thickness, etc.), the presence of residual charge leads to no significant difference ($\leq \pm 10\%$) in the SHG intensity. Infrequently, after subjecting the film to the corona discharge at high fields, an opaque halo could be detected visually on the surface of the film. The impact of corona poling on the film was readily observed in the optical absorption spectrum (Figure 5). The postpoling spectrum reveals a notable reduction in the peak intensity, a slight band broadening, and a small red (electrochromic) shift (ca. 3 nm) in the band position. Similar electric field-induced changes in film optical spectra have been observed previously[11,20,64] and are attributable to partial orientation of the chromophore molecules, hence the net charge-transfer transition dipole, along the surface normal. The absence of new peaks in the optical absorption spectrum subsequent to poling argues that no decomposition/chemical degradation has occurred.[55]

X-ray diffraction was employed to assess the degree of film ordering/crystallinity as a function of processing conditions. The XRD study was performed on poled (or unpoled) (1–3 μm) (S)-NPP–PHS films which were solvent cast onto ITO–glass substrates. Importantly, the diffraction patterns for the annealed, corona-poled films show few features not attributable to the ITO substrate. Only two broad, low-angle reflections at $2\theta \approx 6°$ and 10° are observed. Such a result is typical of amorphous vitreous materials,[65,66] with the broad, low-angle reflections arising from isolated regions of short-range order.[67]

Values of the second harmonic coefficient, d_{33}, for corona-poled (S)-NPP–PHS films over a wide range of functionalization levels are tabulated in Table 3. These essentially nonresonant values, particularly at the highest functionalization level (79×10^{-9} esu or 32 pm/V at λ = 1.064 μm), rival or exceed many previously reported for *off-resonance SHG measurements* on other side-chain functionalized NLO polymers employing a wide variety of backbones and appended chromophores.[11,16–22]

In regard to how d_{33} varies with polymer architecture, the "chromophore gas" model (eq 2) describes the

$$d_{33} = \frac{1}{2} N f^{2\omega} f^{\omega} f^{\omega} \beta_{zzz} L_3(p) \qquad \text{where } p = f^0 \mu E_p / kT \quad (2)$$

response of noninteracting, uniaxial (*i.e.*, rodlike molecules with the dipole moment axis directed along the long molecular axis) NLO chromophores (*i.e.*, isolated molecules) when under the influence of an electric field.[13] Here, N is the chromophore number density, the f's are local field factors at the indicated frequencies, β_{zzz} is assumed to be the only nonzero component of the molecular hyperpolarizability tensor (β), μ is the chromophore dipole moment, E_p is the poling field strength, and L_3 is the third-order Langevin function, which is proportional to the angular average, $\langle \cos^3 \theta \rangle$. It is this third moment of cos θ which describes the degree of polar order (θ here is the polar angle between the chromophore dipole axis and the surface normal, the direction of the applied field) achieved during electric field poling. The applicability of this model to real NLO systems is an important question and may be addressed in a variety of ways including synthesis, as well as linear and NLO spectroscopy. As can be seen in Figure 9, the relationship between d_{33} and the chromophore number density is nearly linear over the widest range of chromophore number densities yet examined.[11] This finding argues against the importance of chromophore–chromophore aggregation in determining NLO response, even at the highest chromophore number densities—90% functionalized (S)-NPP–PHS, where $N = 22.5 \times 10^{20}$ cm^{-3} (for comparative purposes, the chromophore number density in crystalline NPPOH is calculated from crystallographic data[44] to be 37.0×10^{20} cm^{-3}). Centrosymmetric NPP aggregation would be expected to decrease the observed SHG intensity. As an additional probe of possible microscopic chromophore–chromophore interactions at high NPPOH substitution levels, the bulk NLO properties of a polymer functionalized with *racemic* NPPOH were also investigated. As shown in Figure 9, *the d_{33} value of 75% functionalized, racemic (R) + (S)-NPP–PHS does not deviate significantly from the linear relationship established between d_{33} and N for (S)-NPP–PHS*. These results are a further demonstration of the absence of significant centrosymmetric chromophore aggregation effects on the NLO response of poled (S)-NPP–PHS films.

Equation 2 also predicts that d_{33} should be linear with respect to the electric poling field strength, E_p, at low poling fields. The validity of this relationship is difficult to assess with the corona poling technique, since a precise determination of the electric field strength is not readily obtained. By employing contact poling, however, the assessment can be made. As shown in Figure 10, which depicts experiments using 48% functionalized (S)-NPP–PHS, there is a linear relationship between the two parameters at low to modest field strengths. Equation 2 also predicts that the dependence of d_{33} (which is proportional to $\langle \cos^3 \theta \rangle$) on the dc poling field should be nonlinear (*i.e.*, saturates) at fields greater than ~1.3 MV/cm. The theoretical behavior of $\langle \cos^3 \theta \rangle$ as a function of field strength, as predicted by eq 2, is illustrated in Figure 11. The agreement with experiment is excellent.

SHG Temporal Characteristics. All poled chromophoric glassy polymer ensembles are thermodynamically unstable. Therefore, upon field removal, chromophore relaxation will erode the poling-induced noncentrosymmetry and hence limit SHG temporal stability. Temporal stability characteristics of the second harmonic coefficients, d_{33}, were measured for the

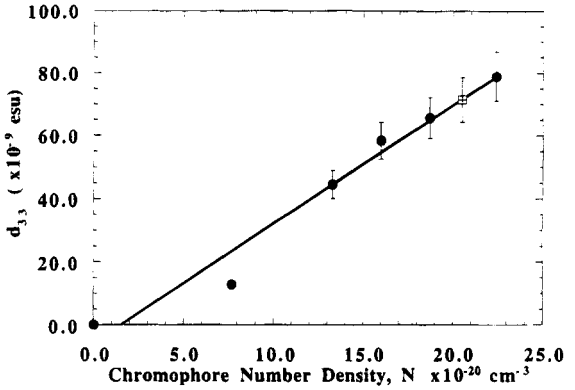

Figure 9. Second-order nonlinear optical coefficient, d_{33}, of poled NPP–PHS films as a function of the chromophore number density, N, at a constant field strength. The solid circles correspond to data for (*S*)-NPP–PHS; the square corresponds to data for *racemic* NPP–PHS. The line is a linear regression fit to the data.

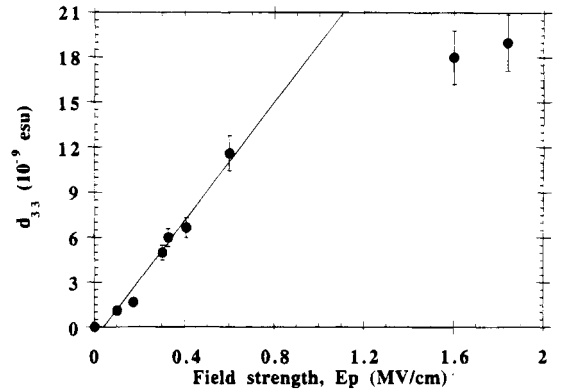

Figure 10. Second-order nonlinear optical coefficient, d_{33}, as a function of the applied contact poling field strength for contact-poled samples of 48% functionalized (*S*)-NPP–PHS (poled at 110 °C). The line represents a linear regression fit to the low-field data.

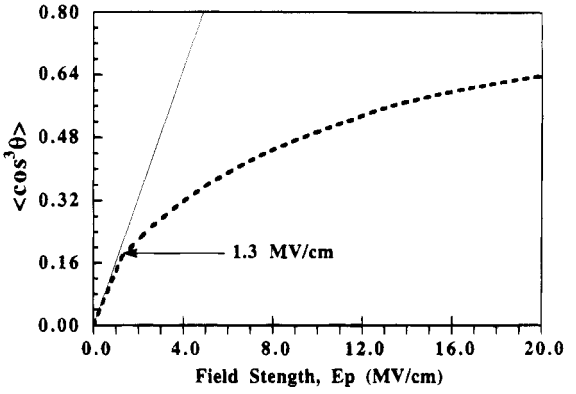

Figure 11. Theoretical poling field-dependent behavior of $\langle\cos^3\Theta\rangle$ ($\propto d_{33}$; dashed line) as predicted by eq 2. Calculation parameters: $\mu = 2.34 \times 10^{-29}$ C m, $T = 423$ K. Approximate linearity up to a poling field of ~1.3 MV/cm is demonstrated by linear regression analysis (solid line), in agreement with the experimental data of Figure 10.

(*S*)-NPP–PHS polymers and could be fit by nonlinear least-squares analysis to the phenomenological biexponential expression of eq 3. Here, τ_1 and τ_2 refer to

$$d_{33}(t) = A\exp(-t/\tau_1) + B\exp(-t/\tau_2) \qquad (3)$$

average short-term and long-term relaxation times, respectively. (Typically, second harmonic coefficients

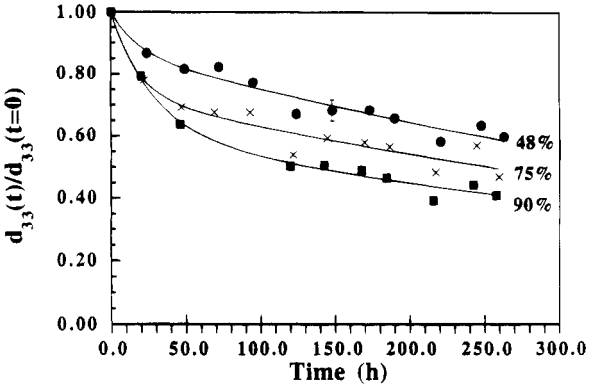

Figure 12. Effect of the functionalization level on the SHG temporal characteristics of poled (*S*)-NPP–PHS films. Samples were corona-poled at 133 °C and +3.4 kV. Curves represent least-squares fits to a biexponential function (eq 3). A representative error bar is provided on the 48% (*S*)-NPP–PHS transient. Decay measurements were taken at 25 °C.

Table 4. Effect of Chromophore Functionalization Level on the Temporal Characteristics of the Second Harmonic d_{33} Coefficient[a]

functionalization level (%)	τ_1 (h)	τ_2 (h)	A	B
48	61.0 (9.0)	1321.8 (164.6)	0.27 (0.03)	0.73 (0.01)
75	38.0 (7.1)	864.5 (92.0)	0.32 (0.1)	0.68 (0.1)
90	26.5 (2.4)	690.4 (43.1)	0.40 (0.05)	0.60 (0.05)

[a] Fit parameters were obtained by fitting data (Figure 12) to eq 3.

normalized to unity at $t = 0$ are fit. Thus, the sum of the coefficients A and B is equal to 1). Alternative models exist to describe the observed relaxation behavior, among them the Kolhrausch–Williams–Watts (KWW) expression, which describes the behavior as a manifold of relaxation processes.[11,38,68] The biexponential function was elected for use here since it provides a convenient way to express the temporal characteristics as a biphasic process, possessing short- and long-term relaxation times.[69,70] This "two-state" description of chromophore relaxation after electric field poling provides an indication of the microenvironment of the encapsulated chromophores within the polymer matrix. That is, application of the free volume model of Cohen and Grest[71] permits association of the fast relaxation component with facile rotational diffusion of the chromophore in "liquid-like" microvoids, while the slower relaxation component is associated with restricted chromophore motion in "glass-like" islands. A formal derivation and physical interpretation of a bimodal functional form will be presented in detail elsewhere.[72]

The effect of NPP functionalization level on SHG temporal characteristics is presented in Figure 12. Each of the samples was corona poled at 133 °C (*i.e.*, above T_g) using an applied voltage of +3.4 kV. Once steady-state (*i.e.*, saturation) SHG intensity was reached, the films were cooled to room temperature and physically aged for 1.0 h prior to field removal. Qualitatively, the results show that the disorientation of the imposed alignment is more rapid at higher levels of chromophore functionalization. Fitting the data to a biexponential function reveals that the decay rates differ in both the short-term and long-term decay components and that both τ_1 and τ_2 increase with decreasing functionalization levels (Table 4). The increase in the rate of decay with increased chromophore number density can be qualitatively correlated with the dependence of T_g on function-

alization level (Figure 8). As noted above, this diminution in T_g with side-chain functionalization is typical of amorphous random copolymers exhibiting a single T_g intermediate between the T_g's of the constituent monomer units (cf. eq 1). For poled (*S*)-NPP–PHS films, the lower T_g values are clearly associated with more facile chromophore reorientation to an isotropic microstructure once the poling field is terminated.

As stated previously, inclusion of extraneous low molecular weight components in a polymer matrix can act adversely as plasticizers. Since these small molecular components (*e.g.*, THF) are volatile, however, they can be readily removed using the previously described high-temperature annealing procedure. The effect of this annealing procedure upon the decay characteristics of a typical sample is shown in Figure 13. A comparison of curve A, for an annealed 12% functionalized NPP–PHS (τ_2 = 133 days) film with curve B, an unannealed film sample (τ_2 = 84 days), demonstrates that chromophore reorientation can be further inhibited by using this processing method. The annealing procedure serves primarily to reduce the initial decay feature (τ_1) characteristically found in poled polymer second harmonic decay curves.

Simultaneous Poling and Cross-Linking. Cross-linking was investigated as a means of further improving the temporal characteristics of poling-induced acentricity the chromophore-functionalized polymer. Although this approach has now been employed by a number of groups,[11,21,74–76] the critical parameters involved have not been investigated in detail. In the present study, the matrix is simultaneously poled and vitrified/cured with a polyfunctional epoxide reagent.[77] The question concerns what procedures most effectively immobilize the preferentially aligned chromophore substituents. Several model diepoxides having differing degrees of chain flexibility and distances between the reactive groups were examined as crosslinking agents (**II**–**IV**). Ideally, the diepoxide should both form inter-

II

III (DEO)

IV (BDE)

chain ether linkages (*i.e.*, between backbone–backbone phenolic groups) and generate new hydroxyl groups, thereby reestablishing sites for hydrogen bonding (Figure 14). The cross-linking process typically is a complex function of multiple variables including temperature, curing time, stoichiometry, and the cross-linking agent.[77,79] In the present studies, optimum conditions (e.g., temperature and time) for the thermal cross-linking were established by FT-IR spectroscopy of (*S*)-NPP–PHS/diepoxide thin films cast onto KBr plates. Cross-linking can be assayed by diminution of the epoxy ring vibrational mode at 913–907 cm^{-1} [79,80] and the concurrent appearance of an ether C–O stretch at 1048–1040 cm^{-1} [79,80] (*e.g.*, Figure 15). Evidence of the cross-linking reaction is observed after heating the film at 60 °C for 1 h (Figure 15B). After 6.5 h at 80 °C, the 907 cm^{-1} band is greatly diminished and the intensity

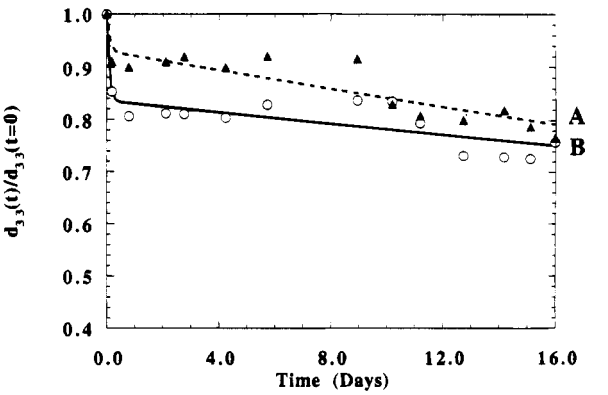

Figure 13. Effect of the annealing procedure on the SHG temporal characteristics of a corona-poled (*S*)-NPP–PHS film: (A) Annealed 12% functionalized (*S*)-NPP–PHS. (B) Unannealed 12% functionalized (*S*)-NPP–PHS. Curves represent nonlinear least-squares fits to eq 3.

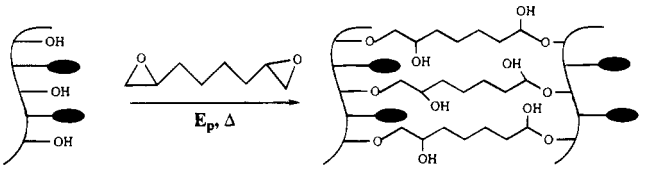

Figure 14. Scheme illustrating the introduction of covalent bonds (cross-links) between polymer chains.

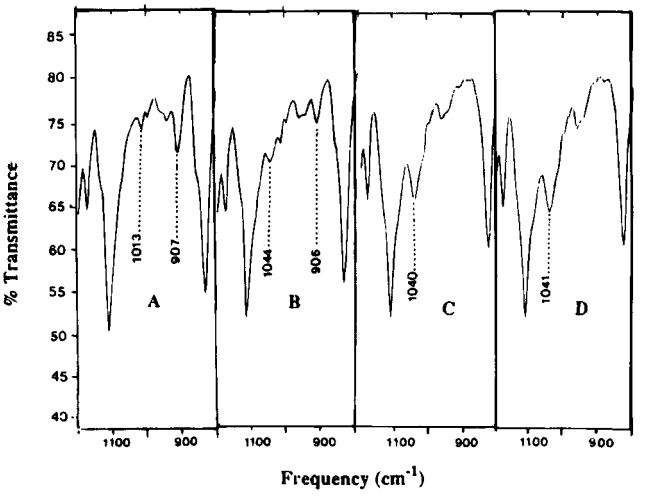

Figure 15. (A) FT-IR spectrum of 16% functionalized (*S*)-NPP–PHS + 1,4-butanediol diglycidyl ether (BDE; **IV**). (B) FT-IR spectrum of 16% functionalized (*S*)-NPP–PHS + 1,4-butanediol diglycidyl ether (BDE) after 1 h of heating at 60 °C. (C) FT-IR spectrum of 16% functionalized (*S*)-NPP–PHS + 1,4-butanediol diglycidyl ether (BDE) after 6.5 h of heating at 80 °C. (D) FT-IR spectrum of 16% functionalized (*S*)-NPP–PHS + 1,4-butanediol diglycidyl ether (BDE) after 14.5 h of heating at 100 °C.

of the 1040 cm^{-1} band substantially increased (Figure 15C). When a film heated for 6.5 h at 80 °C was subsequently heated to 100 °C for 14.5 h, no further change in the spectrum could be detected (Figure 15D). As a result, the cross-linking reaction was considered to be essentially complete after 6.5 h at 80 °C.

Optimum cross-linking stoichiometry and its effect on SHG stability were also investigated. Films of 16% functionalized (*S*)-NPP–PHS containing varying amounts of 1,4-butanediol diglycidyl ether (BDE) were precured at 100 °C for 1 h under an inert atmosphere followed by further heat treatment under vacuum for 24 h. The precured and annealed films were then corona poled at 180 °C for 1 h, cooled to room temperature, and

Table 5. Effect of BDE (IV) Diepoxide Cross-Linker Concentration of the Second-Order Nonlinear Optical Coefficient, d_{33}, and Temporal Characteristics of Corona-Poled 16% Functionalized (S)-NPP–PHS Films

diepoxide	equiv of diepoxide	d_{33} (10^9 esu)	τ_1[a] (days)	τ_2[a] (days)
none	0	8.8	26	30
BDE	0.25	3.8	18	74
BDE	0.50	5.5	20	53
BDE	0.75	2.1	11	51
BDE	1.00	1.4	9	46

[a] Values as determined by least-squares fits to a biexponential function (eq 3).

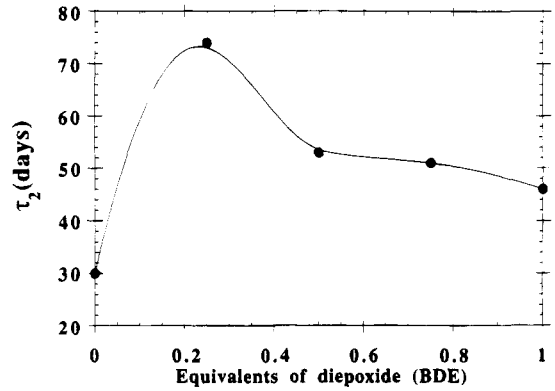

Figure 16. Effect of the BDE diepoxide-to-available phenol OH ratio on the long-term relaxation time constant, τ_2 (eq 3), of (S)-NPP–PHS films simultaneously corona poled and crosslinked. The line is drawn as a guide to the eye.

physically aged for 1 h prior to field removal. The results of this study show (Table 5) that the long-term decay constant, τ_2, is enhanced at even relatively low diepoxide/available phenol OH ratios. In addition, the τ_2 values falls gradually at the higher ratios. This same trend is also observed in τ_1, the short-term decay behavior. The effect of the diepoxide-to-available phenol OH ratio on τ_2 is summarized in Figure 16. The reduction in the relaxation time at higher diepoxide contents can be attributed to unreacted epoxide functionalities (*i.e.*, incomplete cross-linking) which plasticize the chromophore–polymer matrix. At diepoxide stoichiometries greater than 0.5 equiv per phenolic OH, the cross-linked films become opaque after the casting, precuring, and annealing procedure, suggesting phase separation. This leads to a substantial reduction in the measured d_{33}.

Except for the relatively volatile diepoxide **II**, all of the diepoxides investigated provided extensively cross-linked films of high optical quality as judged from FT-IR data and visual inspection. The influence on $d_{33}(t)$ of thermal cross-linking 16% functionalized (S)-NPP–PHS with 0.5 equiv of 1,2,7,8-diepoxyoctane (**III**; DEO) is shown in Figure 17. The decay profile for the uncross-linked or 16% PHS–NPP, curve B, was found to have an average long-term decay constant, τ_2, of 30 days. This is in sharp contrast to the result, curve A, obtained for the cross-linked system where a significant ca. 3-fold enhancement is found in the τ_2 parameter. Figure 18 depicts the effects of thermal cross-linking by a more flexible cross-linker, 1,4-butanediol diglycidyl ether (**IV**; BDE), on the SHG decay characteristics of 12% (S)-NPP–PHS. Interestingly, cross-linking in this case effects an increase in τ_2 of only 275 days → 287 days. This rather modest enhancement in SHG temporal stability may be attributed to the differences in cross-link chain flexibility of the two diepoxides, since

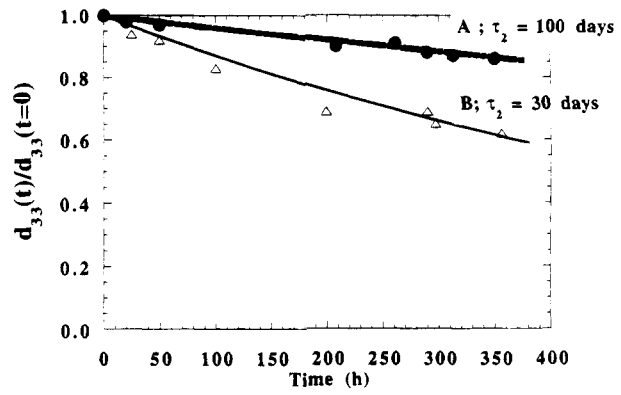

Figure 17. Temporal characteristics of the second harmonic coefficient, d_{33}, for corona-poled (S)-NPP–PHS films. (A) Simultaneously poled at 130 °C and crosslinked with 0.5 equiv of DEO (**III**). (B) Poled at 130 °C. The curves represent nonlinear least-squares fits to eq 3.

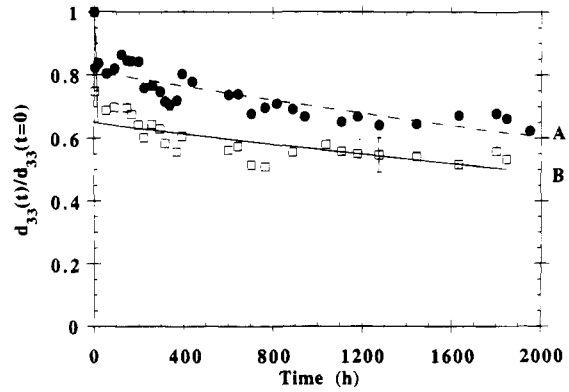

Figure 18. Temporal characteristics of the second harmonic coefficient, d_{33}, for a corona-poled (S)-NPP–PHS film. (A) Simultaneously poled (148 °C) and crosslinked with 0.5 equiv of BDE (**IV**). (B) Poled at 148 °C. Representative error bars provided on data in curve B. Curves represent nonlinear least-squares fits to eq 3.

mobilities of epoxy networks depend on both the cross-link density and the cross-link chain flexibility.[80,81]

Conclusions

The influence of architectural and processing variables on the properties of a broad series of chiral chromophore-functionalized glassy polymers, (S)-NPP–PHS, has been probed by linear optical spectrophotometry, NLO spectroscopy (SHG), FT-IR, and optical rotation measurements. Optical spectra of polymer solutions exhibit, at most, slight saturation of the NPP CT band at the highest functionalization level (90%), arguing against major electronic interaction/structural aggregation of the chromophore moieties. Optical rotation measurements yield essentially the same result. Measurements of the second harmonic coefficient, d_{33}, as a function of chromophore number density in both homochiral and racemic NPP–PHS films are also consistent with minimal NLO-active chromophore aggregation. It seems reasonable to expect that such effects are not confined to the (S)-NPP–PHS polymer. Unfortunately, similar data for other NLO-active chromophore–polymer systems are not adequate to permit comparisons, since most studies have emphasized effects of chromophore or backbone modification rather than systematically investigating the effects of the chromophore functionalization level.

Although the chromophore–chromophore interactions at high NPP–PHS functionalization levels are not

sufficient to degrade the magnitude of d_{33}, an increase in the rate of chromophore relaxation subsequent to cessation of electric field poling is observed. This increase can be correlated with diminution of T_g, and the disruption of the hydrogen-bonding network (detected in the FT-IR) which accompanies increasing substitution levels of NPP for OH groups on the PHS backbone.[82] This observation is further supported by studies on poly(*p*-hydroxystyrene) functionalized with 35% and 88% HNPP (**V**), a chromophore which possesses an additional OH functionality.[74e] Specifically, comparison of the results for HNPP–PHS[74e] to those obtained for NPP–PHS indicates that, at low functionalization levels, the T_g values for the two polymers are nearly the same (137 vs 134 °C). At the highest functionalization level (90%), however, the T_g of NPP–PHS drops to 96 °C. For HNPP–PHS, when hydrogen bonding is possible in spite of chromophore substitution, the decrease in T_g is less dramatic (to 114 °C).

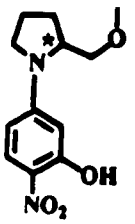

V

NPP–PHS relaxation characteristics can also be impeded by annealing the films prior to poling. By careful optimization of this procedure, small plasticizing molecules (*e.g.*, residual solvent) within the polymer matrix can be effectively eliminated. This procedure may also serve to reduce the average available void volume within the polymer matrix, thereby increasing the steric hindrance to rotation. Contrary to previous reports, the results presented here demonstrate that optimizing the prepole annealing procedure not only functions to reduce the initial decline in SH signal but also acts to significantly enhance retention of the long-term nonlinearity. Unlike many guest–host polymer systems,[85,86] the covalently functionalized NPP–PHS system has been shown to be insensitive to thermal degradation/evaporation of the chromophore from the matrix, even under the rigorous annealing conditions used. Finally, poling in concert with thermal epoxy cross-linking using relatively rigid reagents at optimized stoichiometries is found to substantially enhance the orientational stability of the aligned chromophore substituents, by forming ether linkages between the polymeric chains and reestablishing hydroxyl groups for hydrogen bonding. This produces a dense, three-dimensional network of covalent bonds which restrict the freedom of chromophore motion, thereby enhancing SHG temporal stability characteristics. The present study employed model, *difunctional* epoxy reagents for cross-linking. We show elsewhere that considerable additional enhancements in T_g and SHG temporal stability (≤10% decay over 1000 h at 100 °C) are achievable with improved curing methodologies and *polyfunctional* epoxy cross-linking agents.[85]

In the accompanying paper,[38] we extend our study of this model chromophore-functionalized NLO polymer system to an investigation of appended chromophore and macromolecular dynamics using reorientation transients under sequentially varied poling and processing conditions (*e.g.*, temperature, physical aging, and field strength) to test the applicability of various polymer chain dynamic models.

Acknowledgment. We thank NSF (Grant DMR 9120521 through Northwestern University Materials Research Center) and AFOSR (Contract 93-1-0114) for support of this research. M.A.F. thanks IBM for a Predoctoral Fellowship. We thank Mr. S. B. Roscoe for assistance with the ellipsometry measurements.

References and Notes

(1) Burland, D. M., Ed. Optical Nonlinearities in Chemistry, *Chem. Rev.* **1994**, *94*.
(2) *Molecular Nonlinear Optics: Materials, Physics, and Devices*; Zyss, J., Ed.; Academic Press: Boston, 1993.
(3) *Polymers for Lightwave and Integrated Optics Technology and Applications*; Nornak, L. A., Ed.; Marcel Dekker, Inc.: New York, 1992.
(4) Prasad, P. N.; Williams, D. J. *Nonlinear Optical Effects in Molecules & Polymers*; John Wiley & Sons: New York, 1991.
(5) *Organic Molecules for Nonlinear Optics and Photonics*; Messier, J., Kajzar, F., Prasad, P., Eds.; Kluwer Academic Publishers: Boston, 1991; Vol. 194.
(6) *Materials for Nonlinear Optics: Chemical Perspectives*; Marder, S. R., Sohn, J. E., Stucky, G. D., Eds.; American Chemical Society: Washington, DC, 1991; Vol. 455.
(7) *Nonlinear Optical Effects in Organic Polymers*; Messier, J., Kajar, F., Prasad, P. N., Urlich, D., Eds.; Kluwer Academic Publishers: Dordrecht, The Netherlands, 1989.
(8) *Organic Materials for Nonlinear Optics*; Hann, R. A., Bloor, D., Eds.; Royal Society of Chemistry: London, 1988.
(9) Möhlmann, G. R., Ed. *Nonlinear Optical Properties of Organic Materials. IV. SPIE Proc.* **1993**, *2025*.
(10) Williams, D. J., Ed. *Nonlinear Optical Properties of Organic Materials V. SPIE Proc.* **1992**, *1775*.
(11) (a) Burland, D. M.; Miller, R. D.; Walsh, C. A. Reference 1a, pp 31–75 and references therein. (b) Marks, T. J.; Ratner, M. A. *Angew. Chem., Int. Ed. Engl.*, in press.
(12) Meredith, G. R.; Van Dusen, J. G.; Williams, D. J. *Macromolecules* **1982**, *15*, 1385–1389.
(13) (a) Small, K. D.; Singer, K. D.; Sohn, J. E.; Kuzyk, M. G. *J. Appl. Phys. Lett.* **1986**, *1986*, 248–250. (b) Singer, K. D.; Sohn, J. E.; Lalama, S. J. *J. Appl. Phys. Lett.* **1986**, *49*, 248–250. (c) Singer, K. D.; Kuzyk, M. G.; Sohn, J. E. *J. Opt. Soc. Am. B* **1987**, *4*, 968–975.
(14) (a) Valley, J. F.; Wu, J. W.; Ermer, S.; Stiller, M.; Binkley, E. S.; Kenney, J. T.; Lipscomb, Lytel, R. *Appl. Phys. Lett.* **1992**, *60*, 160–162. (b) Wu, J. W.; Valley, J. F.; Stiller, M.; Ermer, S.; Binkley, E. S.; Kenney, J. T.; Lipscomb, Lytel, R. *SPIE Proc.* **1991**, *1560*, 196–205. (c) Wu, J. W.; Binkley, E. S.; Kenney, J. T.; Lytel, R.; Garito, A. F. *J. Appl. Phys.* **1991**, *69*, 7366–7368. (d) Wu, J. W.; Valley, J. F.; Ermer, E. S.; Binkley, E. S.; Kenney, J. T.; Lipscomb, Lytel, R. *Appl. Phys. Lett.* **1991**, *58*, 225–227.
(15) (a) Hampsch, H. L.; Yang, J.; Wong, G. K.; Torkelson, J. M. *Macromolecules* **1988**, *21*, 526–528. (b) Hampsch, H. L.; Yang, J.; Wong, G. K.; Torkelson, J. M. *Polym. Commun.* **1989**, *30*, 40–43. (c) Hampsch, H. L.; Yang, J.; Wong, G. K.; Torkelson, J. M. *Macromolecules* **1990**, *23*, 3640–3647. (d) Hampsch, H. L.; Yang, J.; Wong, G. K.; Torkelson, J. M. *Macromolecules* **1990**, *23*, 3648–3654. (e) Schüssler, S.; Richert, R.; Bässler, H. *Macromolecules* **1994**, *27*, 4318–4326.
(16) (a) Ye, C.; Marks, T. J.; Yang, J.; Wong, G. K. *Macromolecules* **1987**, *20*, 2322–2324. (b) Ye, C.; Minami, N.; Marks, T. J.; Yang, J.; Wong, G. K. *Macromolecules* **1988**, *21*, 2899–2901. (c) Dai, D. R.; Marks, T. J.; Yang, J.; Lundquist, P. M.; Wong, G. K. *Macromolecules* **1990**, *23*, 1891–1894. (d) Ye, C.; Minami, N.; Marks, T. J.; Yang, J.; Wong, G. K. Reference 7, pp 173–183.
(17) Singer, K. D.; Kuzyk, M. G.; Holland, W. R.; Sohn, J. E.; Lalama, S. J.; Commizzoli, R. B.; Katz, H. E.; Schilling, M. L. *Appl. Phys. Lett.* **1988**, *53*, 1800–1802.
(18) (a) Eich, M.; Sen, A.; Looser, H.; Bjorklund, G. C.; Swalen, J. D.; Twieg, R.; Yoon, D. Y. *J. Appl. Phys.* **1989**, *66*, 2559–2567. (b) Jungbauer, D.; Terakoka, I.; Yoon, D. Y.; Reck, B.; Swalen, J. D.; Twieg, R.; Willson, C. G. *J. Appl. Phys.* **1991**, *69*, 8011–8017.
(19) (a) Robello, D. R.; Schildkraut, J. S.; Armstrong, N. J.; Penner, T. L.; Köhler, W.; Willand, C. S. *Polym. Prep.* **1991**, *32*, 78,

79. (b) Köhler, W.; Robello, D. R.; Willand, C. S.; Williams, D. J. *Macromolecules* **1991**, *24*, 4689–4699.
(20) (a) Mortazavi, M. A.; Knoesen, A.; Kowel, S. T.; Higgins, B. G.; Dienes, A. *J. Opt. Soc. Am. B* **1989**, *6*, 733–741. (b) Mortazavi, M. A.; Knoesen, A.; Kowel, S. T.; Henry, R. A.; Hoover, J. M.; Lindsay, G. A. *Appl. Phys. B* **1991**, 287–295. (c) Lindsay, G. A.; Henry, R. A.; Hoover, J. M.; Knoesen, A.; Mortazavi, M. A. *Macromolecules* **1992**, *25*, 4888–4894.
(21) (a) Xu, C.; Wu, B.; Todorova, O.; Dalton, L. R.; Shi, Y.; Ranon, P.; Steier, W. H. *Macromolecules* **1993**, *26*, 5303–5309. (b) Yu, L.; Chan, W.; Dikshit, S.; Bao, Z.; Shi, Y.; Steier, W. H. *Appl. Phys. Lett.* **1992**, *60*, 1655–1657. (c) Chen, M.; Yu, L.; Dalton, L.; Shi, Y.; Steier, W. H. *Macromolecules* **1991**, *24*, 5421–5428.
(22) Peng, Z.; Yu, L. *Macromolecules* **1994**, *27*, 2638–2640.
(23) Buckley, A.; Riggs, J. P.; Stamatoff, J. B.; Yoon, H. N. Reference 5, pp 447–459.
(24) Hayashi, A.; Goto, Y.; Nakayama, M.; Kaluzynski, K.; Sato, H.; Kato, K.; Kondo, K.; Watanabe, T.; Miyata, S. *Chem. Mater.* **1992**, *4*, 555–562.
(25) Rondou, P.; Van Beylen, M.; Samyn, C. *Makromol. Chem.* **1992**, *193*, 3045–3055.
(26) Cheng, L. T.; Foss, R. P.; Meredith, G. R.; Tam, W.; Zumsteg, F. C. *Mater. Res. Soc. Symp. Proc.* **1992**, *247*, 27–38.
(27) (a) Man, H. T.; Yoon, H. N. *Adv. Mater.* **1992**, *4*, 159–168. (b) Wang, H.; Jarnagin, R. C.; Samuelski, E. T. *Macromolecules* **1994**, *27*, 4705–4713.
(28) Loucif-Saibi, Nakatani, K.; Delaire, J. A.; Dumont, M.; Sekkat, Z. *Chem. Mater.* **1993**, *5*, 229–236.
(29) Page, R. H.; Jurich, M. C.; Reck, B.; Sen, A.; Twieg, R. J.; Swalen, J. D.; Bjorklund, G. C.; Willson, C. G. *J. Opt. Soc. Am. B* **1990**, *7*, 1239–1250.
(30) Chen, M.; Yu, L.; Dalton, L.; Shi, Y.; Steier, W. H. *Macromolecules* **1991**, *24*, 5421–5428.
(31) Hayashi, A.; Goto, Y.; Nakayama, M. *Chem. Mater.* **1991**, *3*, 6–8.
(32) Robello, D. R.; Dao, P. T.; Phelan, J.; Revelli, J.; Schildkraut, J. S.; Scozzafava, M.; Ulman, A.; Willand, C. S. *Chem. Mater.* **1992**, *4*, 425–435.
(33) S'Heeren, G.; Vanermen, G.; Samyn, C.; Van Beylen, M.; Persoons, A. *Mater. Res. Soc. Symp. Proc.* **1992**, *247*, 129–134.
(34) Velsko, S. P. Reference 6, pp 344–359.
(35) Nakamura, K.; Hatakeyama, T.; Hatakeyama, H. *Polymer* **1981**, *22*, 473–476.
(36) Archi, S.; Sakamoto, N.; Yoshida, M.; Himuro, S. *Polymer* **1986**, *27*, 1761–1767.
(37) Brown, W. E. In *Handbook of Plastic Materials and Technology*; Rubin, I. I., Ed.; John Wiley & Sons: New York, 1990; pp 459–485.
(38) Firestone, M. A.; Marks, T. J.; Ratner, M. A.; Lin, W.; Wong, G. K. *Macromolecules* **1995**, *28*, 2260–2269.
(39) Braun, P. *Encyclopedia of Polymer Science and Engineering*; Wiley: New York, 1979; pp 82–83.
(40) Ladd, M. F. C.; Palmer, R. A. *Structure Determination by X-ray Crystallography*, 2nd ed.; Plenum: New York, 1985; p 195.
(41) Tompkins, H. G. *A User's Guide to Ellipsometry*; Academic Press: New York, 1993; pp 3–45.
(42) Dobrowokski, J. A.; Ho, F. C.; Waldorf, A. *Appl. Opt.* **1983**, *22*, 3191–3200.
(43) Ranon, P. M.; Shi, Y.; Steier, W. H.; Xu, C.; Wu, B.; Dalton, L. R. *Appl. Phys. Lett.* **1993**, *63*, 2605–2607.
(44) Zyss, J.; Nicoud, J. F.; Coquillay, M. J. *J. Chem. Phys.* **1984**, *81*, 4160–4167.
(45) Baroukas, M.; Josse, D.; Fremaux, P.; Zyss, J.; Nicoud, J. F.; Morely, J. *J. Opt. Soc. Am. B* **1987**, *4*, 977–986.
(46) Marvel, C. S.; Sekera, V. *C. Org. Synth.* **1955**, *III*, 366, 367.
(47) Comizzoli, R. B. *J. Electrochem. Soc.* **1987**, *134*, 424–429.
(48) (a) VanderVorst, C. P. J. M.; Pickens, J. J. *J. Opt. Soc. Am. B* **1990**, *4*, 918–922. (b) Firestone, M. A.; Lin, W.; Wong, G. K.; Ratner, M. A.; Marks, T. J., manuscript in preparation.
(49) Shirley, D. A.; Ready, W. H. *J. Am. Chem. Soc.* **1951**, *73*, 458, 459.
(50) Poly(*p*-hydroxystyrene) Product Information Bulletin, Hoechst-Celanese Chemical Intermediates Division, Portsmouth, VA.
(51) Kanis, D. R.; Ratner, M. A.; Marks, T. J. *J. Am. Chem. Soc.* **1990**, *112*, 8203, 8204.
(52) Kanis, D. R.; Ratner, M. A.; Marks, T. J.; Zerner, M. *Chem. Mater.* **1991**, *3*, 19–22.
(53) Kanis, D. R., private communication.
(54) (a) Rao, C. N. R. *Ultra-Violet and Visible Spectroscopy*; Butterworths: London, 1967; pp 3 and 4. (b) Harris, D. C. *Quantitative Chemical Analysis*; W. H. Freeman, Co.: New York, 1988; p 501.
(55) Considering the negligible optical cross section of (*S*)-NPP–PHS films at 532 nm and the reasonably anticipated photochemical quantum yields for PHS and NPP photochemical processes as well as the low radiation fluence of the present SHG measurement setup (<10 ns pulse widths; 10 Hz repetition rate), negligible 1064 nm photochemical damage is expected: (a) McKellar, J. F.; Allen, N. S. *Photochemistry of Man-Made Polymers*; Applied Science Publishers: London, 1979; pp 1–2. (b) Kagan, J. *Organic Photochemistry Principle and Applications*; Academic Press: New York, 1993; pp 5–9. (c) Seppon, C. J. E.; Rikken, G. L. J. A.; Staning, E. G. J.; Nrjhuo, S.; Venhuizen, A. *J. Appl. Phys. B* **1991**, *53*, 282–286. Further evidence for negligible photochemistry is provided by the observation that, in long-term SHG decay experiments, the 397-nm NPP charge-transfer band *increases* in intensity (due to depoling) rather than *decreases*, which might be expected if extensive chromophore photochemical damage were occurring.
(56) Willard, H. H.; Merritt, L.; Dean, J. A. *Instrumental Methods of Analysis*, 5th ed.; Van Nostrand: New York, 1974; pp 441–443.
(57) Koenig, J. L. *Spectroscopy of Polymers*; American Chemical Society: Washington, DC, 1992.
(58) Vankrevelen, D. W. *Properties of Polymers*; Elsevier: New York, 1990; pp 314–316.
(59) *Polymer Characterization and Analysis*; Coleman, M. M., Painter, P. C., Eds.; Wiley: New York, 1990; pp 388–390.
(60) Pochert, C. J. *Aldrich Library of IR Spectra*; Aldrich: Milwaukee, WI, 1981; p 139G.
(61) (a) Siesler, H. W.; Holland, T.; Moritz, K. *Infrared and Raman Spectroscopy of Polymers*; Marcel Dekker, Inc.: New York, 1980; pp 150–152. (b) Haaland, D. M. In *Practical Fourier Transform Infrared Spectroscopy: Industrial and Laboratory Chemical Analysis*; Ferraro, J. R., Kushman, K., Eds.; Academic Press: New York, 1990; pp 405–407.
(62) (a) Billmeyer, F. W. *Textbook of Polymer Sciences*, 3rd ed.; John Wiley & Sons: New York, 1984; pp 339 and 340. (b) Nicolson, J. W. *Chemistry of Polymers*; Royal Society of Chemistry: Cambridge, U.K., 1990; pp 54 and 55. (c) Wood, L. A. *J. Polym. Sci.* **1959**, *28*, 319.
(63) Blythe, A. D. *Electrical Properties of Polymers*; Cambridge University Press: London, 1980; pp 150–152.
(64) (a) Swalen, J. D.; Bjorklund, G. C.; Fleming, W.; Hermenghaus, S.; Jungbauer, D.; Jurnis, M.; Moener, W. E.; Reck, B.; Smith, B. A.; Twieg, R.; Willson, C. G.; Zental, R. Reference 3, pp 433–453. (b) Page, R. H.; Jürich, M. C.; Reck, B.; Sen, A.; Twieg, R. J.; Swalen, J. D.; Bjorklund, G. C.; Willson, C. G. *J. Opt. Soc. Am. B* **1990**, *7*, 1239–1250.
(65) Wong, J.; Angell, C. A. *Glass Structure by Spectroscopy*; Marcel Dekker: New York, 1976; pp 53–88.
(66) Roe, R. J. *Encyclopedia of Polymer Science & Engineering*, 2nd ed.; Wiley: New York, 1987; Vol. 17, pp 968–990.
(67) Kampf, G. *Characterization of Plastics by Physical Methods*; Hansen Publishers: New York, 1986; pp 84–109.
(68) Williams, G.; Watts, D. C. *Trans. Faraday Soc.* **1970**, *66*, 80–87.
(69) Yu, W. C.; Sung, C. S. P.; Robertson, R. E. *Macromolecules* **1988**, *21*, 355–364.
(70) Sung, C. S. P.; Gould, I. R.; Turro, N. J. *Macromolecules* **1984**, *17*, 1447–1451.
(71) Cohen, M. H.; Grest, G. S. *Phys. Rev. B* **1979**, *20*, 1077–1085.
(72) Firestone, M. A.; Thachuk, M.; Ratner, M. A.; Marks, T. J., manuscript in preparation.
(73) Fox, T. G. *Bull. Am. Phys. Soc.* **1956**, *1*, 123.
(74) (a) Hubbard, M. A.; Minami, N.; Ye, C.; Marks, T. J.; Wong, G. K. *SPIE Proc.* **1988**, *971*, 136–143. (b) Hubbard, M. A.; Marks, T. J.; Yang, J.; Wong, G. K. *Chem. Mater.* **1989**, *1*, 167–169. (c) Dai, D. R.; Hubbard, M. A.; Park, J.; Marks, T. J.; Yang, J.; Wong, G. K. *Mol. Cryst. Liq. Cryst.* **1990**, *189*, 93–106. (d) Park, J.; Marks, T. J.; Yang, J.; Wong, G. K. *Chem. Mater.* **1990**, *2*, 229–231. (e) Jin, Y.; Carr, S. H.; Marks, T. J.; Lin, W.; Wong, G. K. *Chem. Mater.* **1992**, *4*, 963–965. (f) Hubbard, M. A.; Marks, T. J.; Lin, W.; Wong, G. K. *Chem. Mater.* **1992**, *4*, 965–968. (g) Wang, J.-F.; Hubbard, M. A.; Jin, Y.; Lin, J. T.; Marks, T. J.; Lin, W. P.; Wong, G. K. *SPIE Proc.* **1993**, *2025*, 62–68.
(75) Jungbauer, D.; Reck, B.; Tweig, R.; Yoon, D. Y.; Willson, C. G.; Swalen, J. D. *Appl. Phys. Lett.* **1990**, *56*, 2610–2612.
(76) Jeng, R. J.; Chen, Y. M.; Jain, A. K.; Kumar, J.; Tripathy, S. K. *Chem. Mater.* **1992**, *4*, 1141–1144.
(77) (a) Lohse, F. *Makromol. Chem., Macromol. Symp.* **1987**, *7*, 1–16. (b) Oleinik, E. F. *Adv. Polym. Sci.* **1986**, *80*, 49–99.

(c) Dusek, K. *Adv. Polym. Sci.* **1986**, *78*, 1–59. (d) Rozenberg, B. A. *Adv. Polym. Sci.* **1986**, *75*, 113–165.
(78) McAdams, L. V.; Gannon, J. A. *Encyclopedia of Polymer Science & Engineering*; Wiley: New York, 1986; Vol. 6, pp 322–382.
(79) Mertzel, E.; Koening, J. L. *Adv. Polym. Sci.* **1985**, *75*, 74–112.
(80) Cuikerman, S.; Halary, J. L.; Monnerie, L. J. *J. Non-Crystal. Solids* **1991**, *131*, 898–905.
(81) Kwei, T. K. *Adv. Polym. Sci.* **1966**, *4*, 943–949.
(82) For discussions of the importance of hydrogen bonding in poly(*p*-hydroxystyrene) structure and chain dynamics, see: (a) Moskala, E. J.; Varnell, D. F.; Coleman, M. M. *Polymer* **1985**, *26*, 228–234. (b) Nakamura, A.; Hatakeyama, T.; Hatakeyama, H. *Polymer* **1981**, *22*, 473–476. (c) Hatakeyama, T.; Nakamura, A.; Hatakeyama, H. *Polymer* **1978**, *19*, 593, 594.
(83) Kobayashi, T.; Minoshima, K.; Nomura, S.; Fukaya, U. *SPIE Proc.* **1989**, *1147*, 182–197.
(84) Stahelin, M.; Burland, D. M.; Ebert, M.; Miller, R. D.; Smith, B. A.; Twieg, R. J.; Volksen, W.; Walsh, C. A. *Appl. Phys. Lett.* **1992**, *61*, 1626–1628.
(85) (a) Crumpler, E. T.; Li, D.; Marks, T. J.; Ratner, M. A.; Lin, W.; Wong, G. K. Abstracts of the 207th National Meeting of the American Chemical Society, San Diego, CA, March 13–17, 1994, INOR 521. (b) Crumpler, E. T.; Marks, T. J.; Lin, W. P.; Wong, G. K. *Chem. Mater.*, in press.

MA945012H